# Plasma-wall interaction studies in W7-X: Main results from the recent divertor operations

C P Dhard[1,*], S Brezinsek[2], M Mayer[3], D Naujoks[1], S Masuzaki[4], D Zhao[2], R Yi[2], J Oelmann[2], K Schmid[3], J Romazanov[2, 10], C Pardanaud[5], M Kandler[3], A K Kharwandikar[1], G Schlisio[1], O Volzke[1], H Grote[1], Y Gao[1], L Rudischhauser[1], A Goriaev[6,7], T Wauters[6], A Kirschner[2], S. Sereda[2], E Wang[2], M Rasinski[2], T Dittmar[2], G Motojima[4], D Hwangbo[8], S Kajita[9], M Balden[3], V V Burwitz[3], R Neu[3], Ch Linsmeier[2], and the W7-X Team[1§]

[1]Max-Planck-Institut für Plasmaphysik, Wendelsteinstrasse 1, 17491 Greifswald, Germany
[2]Forschungszentrum Jülich GmbH, Institut für Energie- und Klimaforschung – Plasmaphysik, Partner of the Trilateral Euregio Cluster (TEC), 52425 Jülich, Germany
[3]Max-Plank-Institut für Plasmaphysik, Boltzmannstrasse 2, 85748 Garching, Germany
[4]National Institute for Fusion Science, 322-6 Oroshi, Toki 509-5292, Japan
[5]Aix-Marseille Université, Laboratoire PIIM, 13013 Marseille, France
[6]Laboratory for Plasma Physics, LPP-ERM/KMS, B-1000 Brussels, Belgium
[7]Department of Applied Physics, Ghent University, Ghent, Belgium
[8]Department of Electrical Engineering, Graduate School of Engineering, Nagoya University, Furo-cho, Chikusa, Nagoya 464-8603, Japan
[9]Institute of Materials and Systems for Sustainability, Nagoya University, Furo-cho, Chikusa, Nagoya 464-8603, Japan
[10]JARA-HPC, Jülich Supercomputing Centre, Forschungszentrum Jülich GmbH, 52425 Jülich, Germany
[§]The W7-X Team are the co-authors mentioned in the paper, T. Klinger et al., Nuclear Fusion 59 (2019) 112004

Email: chandra.prakash.dhard@ipp.mpg.de

Wendelstein 7-X (W7-X) is an optimized stellarator with the 3-dimensional five-fold modular geometry. The plasma-wall-interaction (PWI) investigations in the complex 3D geometry of W7-X were carried out by in-situ spectroscopic observations, exhaust gas analysis and post-mortem measurements on a large number of plasma-facing components extracted after campaigns.

The investigations showed that the divertor strike line areas on the divertor targets appeared to be the major source of carbon impurities. After multistep erosion and deposition events, carbon was found to be deposited largely at the first wall components, with thick deposits of >1 μm on some baffle tiles, moderate deposits on toroidal closure tiles and thin deposits at the heat shield tiles and the outer wall panels. Some amount of the eroded carbon was pumped out via the vacuum pumps as volatile hydrocarbons and carbon oxides (CO, $CO_2$) formed due to the chemical processes. Boron was introduced by three boronizations and one boron powder injection experiment. Thin boron-dominated layers were found on the inner heat shield and the outer wall panels, some boron was also found at the TDU and in redeposited layers together with carbon. Local erosion/deposition and global migration processes were studied using field-line transport simulations, analytical estimations, 3D-WallDYN and ERO2.0 modeling in standard magnetic field configuration.

Keywords: Wendelstein 7-X, Plasma-facing components, Plasma-wall interaction, Erosion and deposition, Graphite

## 1. Introduction

Wendelstein 7-X (W7-X) is an optimized three-dimensional helically shaped stellarator with five-fold symmetry designed for steady-state plasma operation of up to 30 min. Since the beginning of W7-X operation with island divertor, there have been two Operation Phases (OP) completed, namely: OP1.2a and OP1.2b. Due to the operational constraints, the total integral energy input during these phases was limited to 80 MJ (OP1.2a) and 200 MJ (OP1.2b), respectively. For OP1.2a PFCs made of fine grain graphite were installed: ten inertially cooled discrete island Test Divertor Units (TDUs), baffles, toroidal divertor closures and wall protection heat shield tiles. The outer wall panels, divertor pumping gap panels, and poloidal closures were made of stainless steel (see figure 1). In addition, for OP1.2b graphite scraper elements were installed near two TDUs in order to mitigate convective plasma heat loads on the

pumping gap panels in certain configurations caused by the evolution of the internal bootstrap current [1-3]. The whole inboard side is covered with graphite heat shield and baffle tiles, whereas stainless steel wall panels cover most of the outboard side of the plasma vessel except at certain locations, e.g., the triangular cross section, where the heat shield tiles are installed as well [4, 5]. The locations of these components are shown in figure 1 and their numbers together with the surface area are given in table 1.

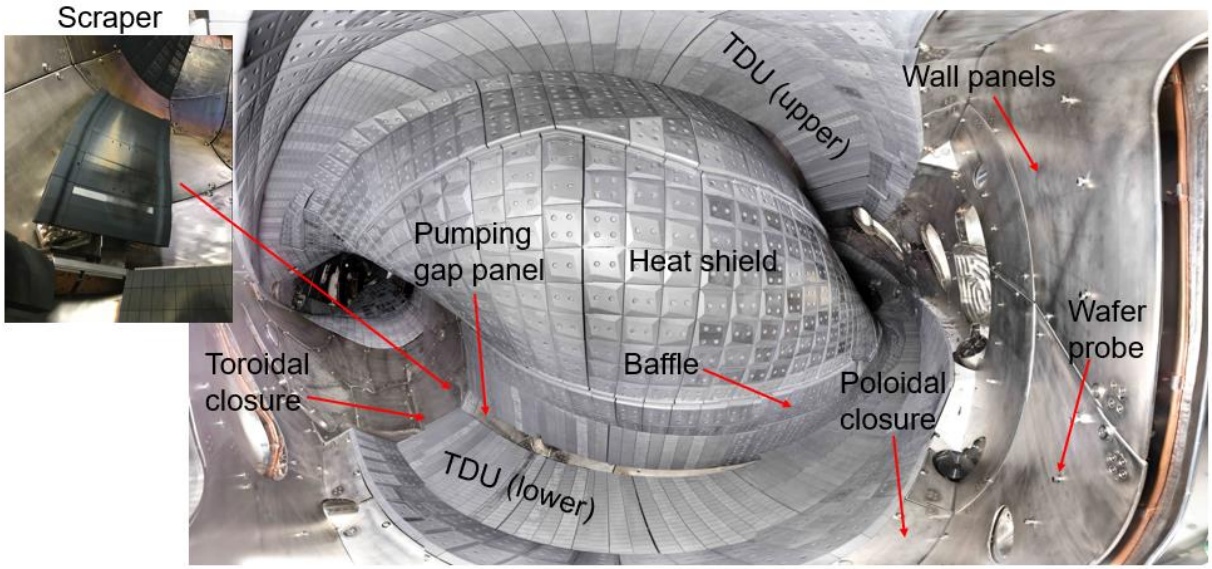


Figure 1. Panoramic view into the W7-X plasma vessel from W7-X module 4, showing the installed plasma-facing components. Figure on the left shows scraper mounted before the toroidal closure along the pumping gap.

Table 1. Surface areas of the W7-X graphite and stainless steel plasma-facing components obtained based on CATIA design data [6].

| **Graphite components** | **Quantity in W7-X** | **Surface area ($m^2$)** | **Stainless steel components** | **No. in W7-X** | **Surface area ($m^2$)** |
|---|---|---|---|---|---|
| TDU-high load | 890 targets | 19 | Wall panel | 200 | 62.3 |
| TDU-low load | 240 targets | 6 | Poloidal closure | 90 | 8.7 |
| Scraper | 12 targets | 0.5 | | | |
| Heat shield | 4460 tiles | 47 | Pumping gap panel | 30 | 6.1 |
| Baffle | 3130 tiles | 33 | | | |
| Toroidal closure | 210 tiles | 3 | | | |
| Port/house protection | | 6.9 | | | |
| Sum | | 115.4 | | | 77.1 |

Carbon (C) migration has been extensively studied in fusion devices with 2-dimensional geometry such as tokamaks equipped with graphite PFCs. In stellarators with their 3-dimensional geometry such studies are much more scarce and ongoing. Due to the profound differences in plasma configuration and the geometry of divertor and other PFCs, the locations of net erosion and net deposition areas could be different. Compared to the Large Helical Device (LHD) [7-10], W7-X provides unique possibilities to study carbon migration in its specific 3-dimensional geometry with modular plasma configurations and island divertors.

Boronization by using the injection of diborane during glow discharge operation is regularly used in fusion machines to suppress oxygen (O) and carbon impurities, resulting in improved plasma operation

[11]. Especially directly after fresh boronizations the plasma-facing surfaces consist mostly of boron rather than carbon and therefore, besides carbon it becomes important to study the plasma-wall interaction and migration of B in these machines. It is also important to investigate the effect of inhomogeneity in the boron distribution on the PFCs on the efficient reduction of oxygen and carbon impurities in the plasma.

Simulations were carried out using Field Line Transport (FLT), WallDYN-3D and ERO2.0 codes in order to interpret the results of the post-mortem surface analyses on selected material probes taken from different positions in W7-X.

The details of the experimental techniques used for the analysis i.e. Elastic Backscattering Spectrometry (EBS), Nuclear Reaction Analysis (NRA), Focused Ion Beam (FIB) cutting, Scanning Electron Microscopy (SEM) and Energy-Dispersive X-ray spectroscopy (EDX) are described in ref. [12], pico-second Laser Induced Breakdown Spectroscopy (ps-LIBS) in ref. [13] and optical reflection measurements in ref. [14].

## 2. Carbon balance

Studying carbon migration in a fusion device with carbon PFCs (graphite) is challenging to quantify by the post-mortem measurements, in particular, the localized erosions or thin depositions with pure carbon layers. For the PWI studies in W7-X, the following two techniques have been applied:

i. Coating the base graphite material with marker layers: 18 targets of the TDU were coated with ca. 0.2 µm of Mo and 5 – 10 µm C marker layers (see figure 2). In order to have a toroidal distribution of erosion/deposition, ten of these were chosen at the same location in each TDU. For the poloidal distribution, eight additional targets were selected on the upper and lower TDU in a single W7-X module (module 5). After OP1.2a, all the 18 targets were exchanged with new similar marker targets [12].

ii. Tungsten coating: 3 tiles of a TDU target, 2 scraper tiles and 21 tiles of the heat shield were coated with thin W layer [15].

iii. Thicker redeposited carbon layers on carbon tiles can be identified using depth-profiling methods by the presence of codeposited hydrogen isotopes or other codeposited impurities, such as oxygen, boron or traces of metals (especially Fe, Ni, Cr). Thin redeposited carbon layers on carbon substrate are generally difficult to quantify and require the use of different substrates.

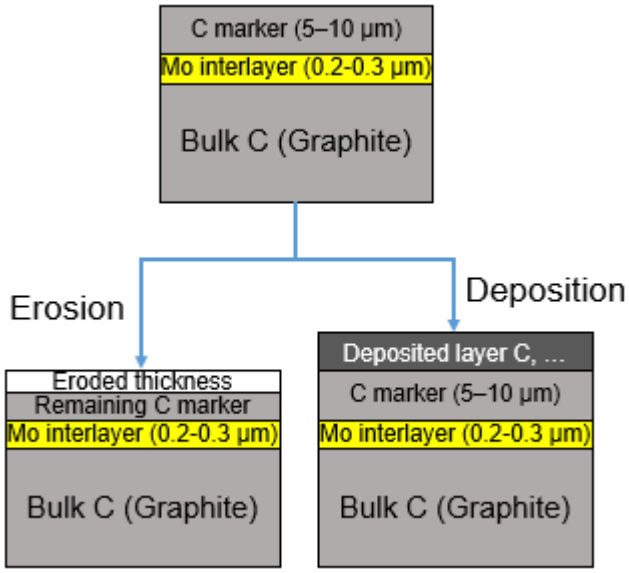


Figure 2. Configuration of marker layer coating on graphite targets and expected result in net erosion and net deposition areas.

Using these techniques, the carbon balance was studies by measuring carbon erosion/deposition at the TDU and deposition at various places after the completion of OP1.2b. The exhaust of volatile carbon-containing molecules via the vacuum pumps was measured by mass spectrometers.

Besides the study of global migration of the carbon eroded from the C-PFCs, to study the local erosion and deposition, a $^{13}C$ isotope was injected in the form of $^{13}CH_4$ on the last day of OP1.2b plasma campaign. A total of 4.2 $x$ $10^{22}$ $^{13}C$ atoms (ca. 0.9 g) were injected (via gas injection nozzles built in the TDU) during 30 consecutive plasma discharges in standard magnetic configuration with identical plasma conditions. Simulations have been performed using 3D codes WallDYN-3D [16] and ERO2.0 [17] to model the erosion and deposition patterns showing good agreement with the initial measurements. A detailed measurements on a number of TDU targets removed after OP1.2b, are under progress, therefore in the present C-balance investigations, the 13C experiments are not included.

### 2.1 Sources of carbon impurities

Based on the post-mortem measurements two different sources for eroded carbon were found:

#### 2.1.1 Erosion on TDU targets

All the 36 targets with the marker layers were analyzed by EBS, some targets were also analyzed by ps-LIBS and SEM/FIB measurements. High erosion at the strike lines was found during OP1.2a such that not only the marker C layer but the underlying Mo interlayer was also eroded. This was due to high concentrations of C and O impurities evident from the high $Z_{eff} \leq 4.5$, resulting in high erosion yields. The total estimated erosion of carbon (for all the TDU) over the whole OP1.2a campaign was 48 ± 14 g yielding a mean erosion rate of 13.9 mg/s [12].

For OP1.2b, three boronizations reduced the C and O impurity concentrations by a factor of 10-100 and resulted in $Z_{eff} \sim 1.5$ [18, 19]. The erosion profile along a typical target shows comparatively lower erosion than in OP 1.2a (see figure 3). Despite of increased plasma duration from 3775 s (OP1.2a) to 9054 s (OP1.2b), the overall erosion of carbon during OP1.2b was reduced to 20 ± 6 g and the erosion rate to 2.3 mg/s.

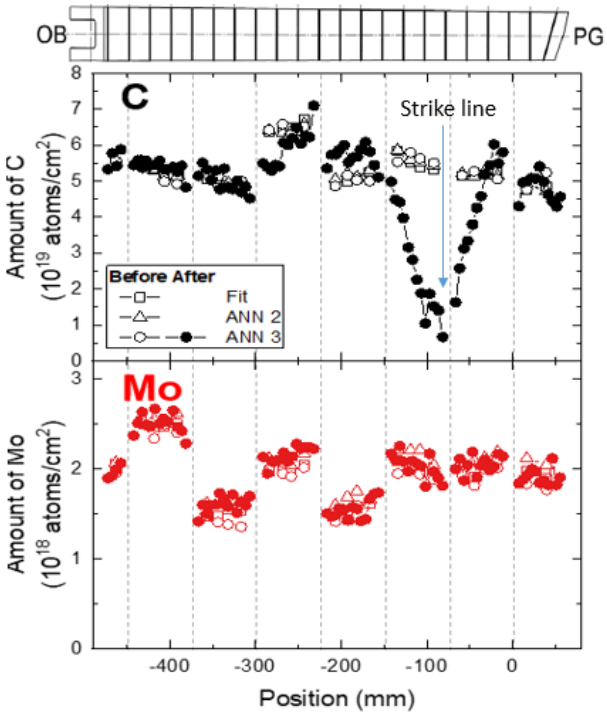


Figure 3. Erosion profile along a TDU target TM2h6 (HM5*l*) for OP1.2b, the measurements of the marker layer thickness before and after the plasma operations are shown for carbon (upper plot) and

Mo (lower plot). The location of plasma strike line is shown by the arrow. ANN represents Artificial Neural Network fittings. The location of pumping gap (PG) is on the right side and the W7-X outboard (OB) on the left side.

### 2.1.2 Glow discharge cleaning

Besides the carbon erosion during the plasma operations, carbon erosion had also occured during the glow discharge cleaning (GDC) operations. For OP1.2, the durations of GDC with He and H gases were 19.64 h and 27.37 h respectively [20]. With the discharge currents of 1 A and 1.5 A, the flux of singly ionized particles for ten GDC electrodes were $6.24 \times 10^{19}$ and $9.36 \times 10^{19}$ ions/s for the He and H ions respectively. Considering the sputtering yields of $\gamma_{He \rightarrow C} = 0.08$ (for GDC voltage 210 eV) and $\gamma_{H \rightarrow C} = 0.009$ (for GDC voltage 305 eV) [21] and ignoring the chemical erosion due to low wall surface temperatures of ca. 30°C, and considering, Area_carbon/(Area_carbon+Area_steel) = 0.6 (=115.4/(115.4+77.1)), the amount of carbon erosions during OP1.2 was $2.12 \times 10^{23}$ ($=6.24 \times 10^{19} \times 0.08 \times 3600 \times 19.64 \times 0.6$) and $4.98 \times 10^{22}$ ($=9.36 \times 10^{19} \times 0.009 \times 3600 \times 27.37 \times 0.6$) C-atoms during He-GDC and H-GDC, respectively. This sums up to a gross-carbon erosion of $2.61 \times 10^{23}$ C-atoms during OP1.2 GDC operations with the total weight of 5.2 g. Considering, the eroded carbon was uniformly redeposited on all the PFCs, the amount of carbon deposited on the stainless steel surfaces would only account as net erosion due to GDC. The ratio of stainless steel areas compared to the total area is 0.4, with the corresponding amount of carbon deposition of **2.1** g. The glow discharge during boronization is not included here, moreover the GDC was suspended after the first boronization due to improved wall conditioning and to avoid sputtering of the thin deposited boron layer.

Considering a homogeneous deposition of the eroded carbon on all the PFC with a total surface area of 192.5 $m^2$ (see table 1) and a density of deposited C-layer as $6.0 \times 10^{28}$ C-atoms/$m^3$, the thickness of the redeposited C-layer works out to be about 22.6 nm ($=2.61 \times 10^{23}/192.5/6.0 \times 10^{28}$), in reality, re-erosion and deposition during the plasma operation will have effects on the observed distribution. However, erosion/deposition during GDCs can reasonably explain the deposition on the plasma vessel wall in the form of stripes as shown in figure 4, where the possibilities of re-erosion by tokamak plasma ions and neutrals was almost negligible. The stripes were formed due to the direct deposition through the small gaps between the carbon heat shield tiles onto the plasma vessel behind. Assuming a uniform distribution behind all the first wall tiles, the estimated area of the deposition stripes is 3.23 $m^2$, the amount of carbon deposition here assuming homogeneous redeposition during GDC is ca. 0.1 g.

The deposition stripes were also found on a TAG number plate mounted on the plasma vessel wall (see figure 4a), which was removed and investigated by EBS for the deposited material. Besides minor B and O deposition, the main deposition was from C atoms with an average surface concentrations of ca. $4.33 \times 10^{21}$ atoms/$m^2$ [22], equivalent to ca. 0.3 g total carbon deposition in the stripes behind the tiles. Within the uncertainties of measurements and the estimations of the areas, this number is of the same order of magnitude with the 0.1 g based on the simplified estimation by considering only the carbon erosion during GDC operations as described above.

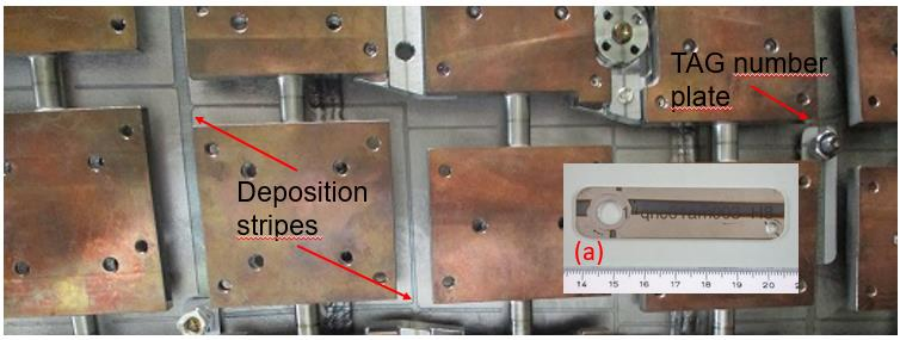


Figure 4. Deposition stripes were formed on the plasma vessel wall by deposition of material through the gap between the graphite tiles. Inset a) shows a TAG number plate mounted on the wall on which the stripes were seen, this was removed for the analysis.

### 2.2 Deposition of carbon

#### 2.2.1 First wall graphite tiles

Out of 7800 graphite tiles in W7-X, about hundred tiles distributed over the torus were removed after OP1.2 for the post-mortem analysis using EBS, ps-LIBS and SEM/FIB/EDX measurements. In particular, thick deposited layers > 1 µm were observed on some baffle tiles installed close to the TDU. As shown in figures 5a and 5b, some of these deposited layers were released in the form of flakes, others are just attached loosely. On the other hand, the depositions on the heat shield and toroidal closure tiles were less pronounced with thicknesses of about 100 nm (see figures 5c and 5d).

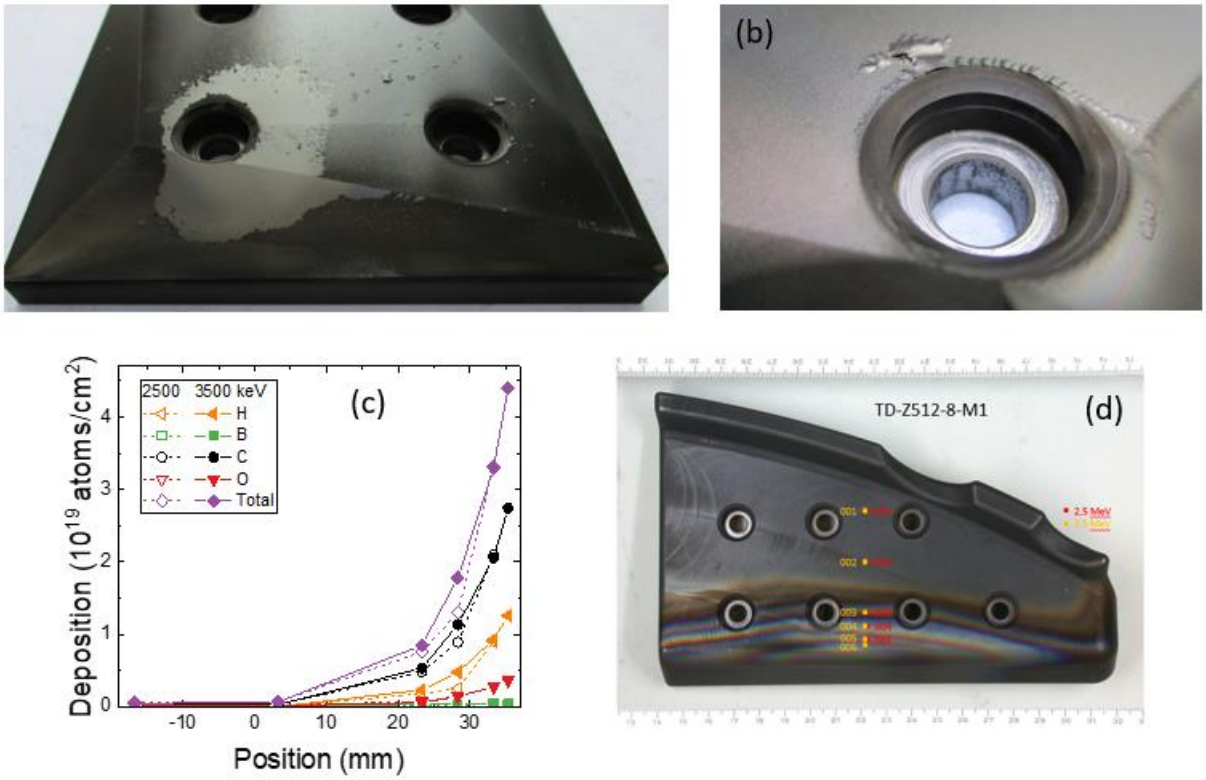


Figure 5. a and b: thick depositions on the baffle tiles, c: EBS measurements on the toroidal closure tile, d: the location of the measurement points on the toroidal closure tile.

Raman spectroscopy is capable of investigating the chemical bonds, defects and structural changes on the surfaces modified by interaction with the incident ions [23]. The measurements, i.e. G band wavenumber ($\sigma_G$) as a function of G band width ($\Gamma_G$) caused by mainly $sp^2$ hybridized C, on the relevant parts of six tiles (tile 7 is from the baffle and the rest from the heat shield) from OP1.2b to test homogeneity of the tiles, are shown in figure 6. Comparison with intensively investigated Tore Supra and pristine CFC samples [24], showed deposition on all these tiles. On tile 2 a small part of area is found close to the erosion region defined by the Tore Supra samples, which would be followed closely after next campaigns.

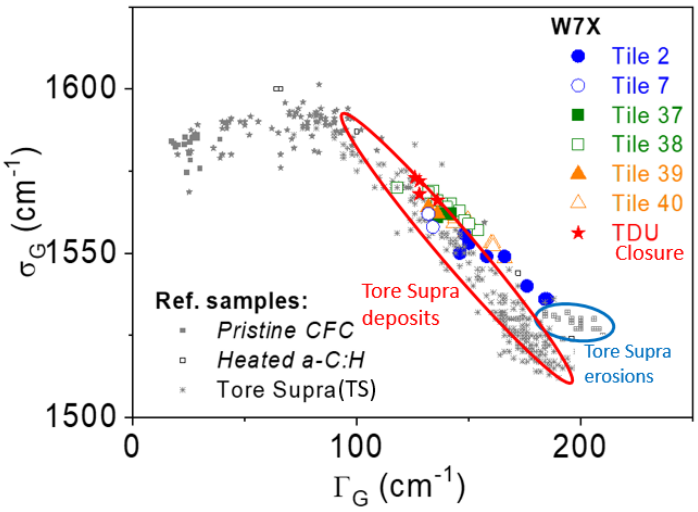


Figure 6. Raman spectroscopy measurements on some of the first wall tiles and their comparison with the Tore Supra samples.

Assuming a uniform deposition on a particular component such as baffle, heat shield and the toroidal closures, the carbon amount deposited on these tiles are estimated using the following relation: tiles (considering the density of deposited C-layers ρ = 1.4 g/cm$^3$)

$$m = \frac{\rho}{t\,A}$$

Here, ρ is the density of deposited C-layer 1.4 g/cm$^3$, $t$ is the average thickness of the deposited layer and $A$ the surface area.

- Baffle: Deposits on baffle tiles are very inhomogeneously distributed and layer thicknesses range from very thin to more than 10 µm. For an estimate of the amount of redeposited carbon we assume an average thickness of 0.5 µm and the surface area of 33 m$^2$ (see table 1) → $m_{\text{baffle}}$=**23 g**
- Heat shield: Deposits on the heat shield were more homogeneous but very thin, which made a precise quantification difficult. We assume an average thickness of 50 nm and the surface area of 47 m$^2$ → $m_{\text{heat shield}}$=**3 g**
- Toroidal closure: average thickness of 50 nm and the surface area of 3 m$^2$ → $m_{\text{toroidal closure}}$=**0.2 g**

The accuracy of these numbers is only within a factor of two.

In general depositions were observed on all these tiles so far indicating absence of erosion zones on the first wall components in OP1.2a and OP1.2b.

### 2.2.2 Carbon deposition on stainless steel panels

The thickness of deposited layers was measured in-situ by an optical reflection (of RGB colors) measurement on the stainless steel panels of the outer wall, poloidal closures and the pumping gap panels after OP1.2a and OP1.2b [14]. Average thicknesses of 10 nm and 15 nm were measured for OP1.2a and 1.2b, respectively. Since these panels cannot be removed for analysis, no specific measurements could be performed for the material concentrations, however, it is expected to be C rich layer for OP1.2a and B/C rich co-deposited layer for OP1.2b. With the surface area of stainless steel PFCs, 77.1 m$^2$ (see table 1) and considering the density of the deposition layer, 1.4 g/cm$^3$, the amount of C works out to be 1.1 g for OP1.2 and B/C co-deposit, 1.6 g for OP1.2b. Assuming equal amounts of B and C deposition, the overall amounts (OP1.2a +OP1.2b) of C would be 1.9 g and B 0.8 g.

### 2.2.3 Dust and arc traces

In the fusion machines with carbon (graphite) plasma-facing components, deposited carbon layers are typically not diamond-like hard layers but loosely bound a-C:H layers with varying hydrogen content due to chemical bonding of C with the fuel atoms. Over periods of operation, once these layers get

thicker, they may get released in the form of flakes or dust particles and may lead to problems in the plasma operation as already observed in Tore Supra [25]. Such dust formations were also observed in other machines i.e. TEXTOR [26] and ASDEX-Upgrade [27]. In W7-X, during the inspection after OP1.2b, 44 samples of dust and loosely bound particles were collected from the TDU, poloidal closures, and the pumping gap at different positions in the torus. However, the amount of dust was found to be very small [22] and does not contribute to the carbon balance significantly. Similarly, the eroded material due to 212 arc traces found on various metal PFCs was also of negligible amount with traces being of micro sizes [22, 28].

### 2.3 Exhaust of volatile carbon oxides and hydrocarbons

Volatile hydrocarbons and oxides (mainly CO and smaller amounts of $CO_2$) formed by the chemical processes occurring during the plasma operations were pumped out via twenty pumping ports, located at the low iota and high iota sides of each TDU. These gases were analyzed using a diagnostic residual gas analyzer (DRGA) at a port in half-module 40. The details of the DRGA measurement set-up (see figure 7) in W7-X are presented in ref. [29].

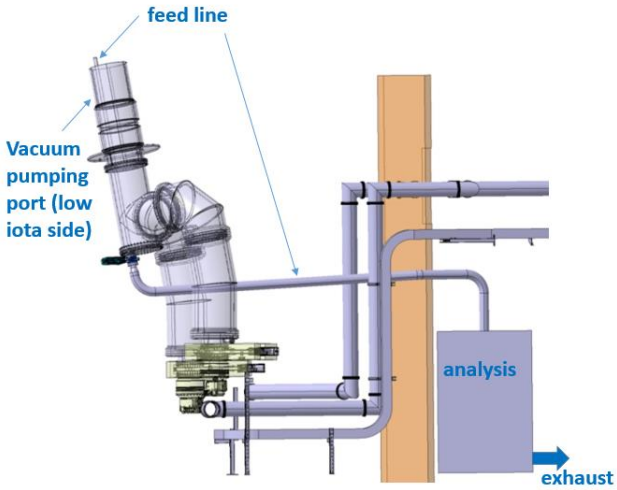


Figure 7. Schematic drawing of the diagnostic residual gas analyzer (DRGA) in W7-X. The feedline is installed in a pumping port on the low iota side in HM 40. The feedline is led to the analyzer unit which is separately pumped.

Two additional mass spectrometers were operated in half-modules 21and 40 but since these were not calibrated, for the present analysis the DRGA data have been used. The amounts of pumped out CO, $CO_2$, $CH_2$ and $CH_4$ are shown for a typical plasma shot 20181004.29 in figure 8. As seen in the figure 8, even though the plasma shot duration was ca. 12 s, the pumped out gases could be measured even until 120 seconds due to the time constant of the vacuum system.

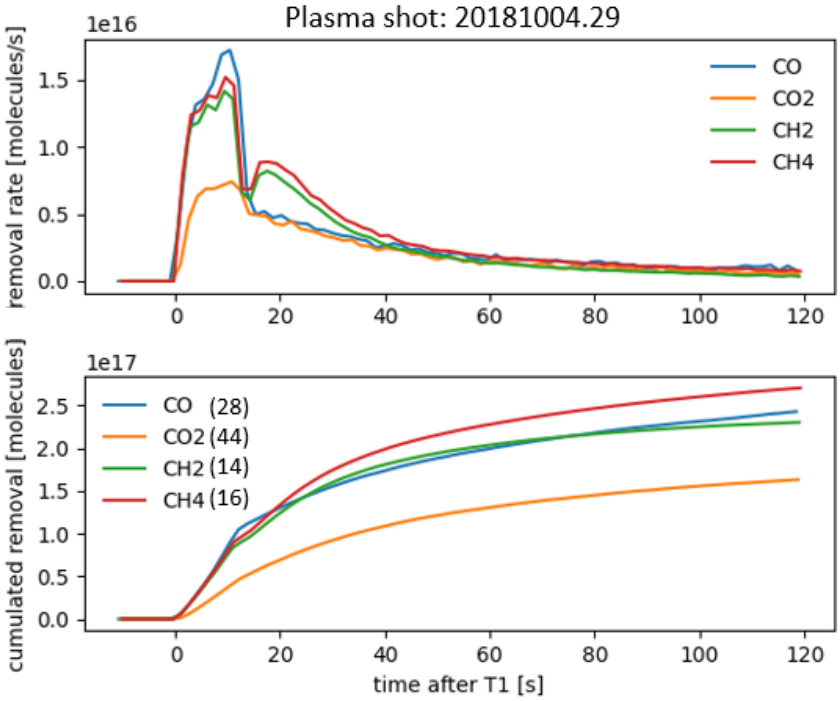


Figure 8. Amounts of pumped out CO, $CO_2$, $CH_2$ and $CH_4$ (with their masses in brackets) during and after the plasma shot 20181004.29. The upper plot shows the removal rate and the lower plot the cumulated amount over time.

The gases measured by the DRGA mass spectrometer are presented in table 2. With the subtraction of background signal, most of the $N_2$ signal was eliminated from the CO (mass 28) signal. It has been considered most of $O_2$ was pumped out in the form of CO and $CO_2$ and no free O was available therefore $CH_4$ denotes mass 16. Assuming the similar amounts in all the ten ports (at the low iota side shown in figure 7) over all the 1256 plasma pulses of OP1.2b, the estimated amounts of gases are shown in table 2. Only the ten ports on low iota side were taken into estimations since more than 80% of the time, the plasma strike lines were on the low iota side of TDU. The chemical erosion on carbon PFCs has been well studied [30-33] and $CH_3$ and $CH_4$ have been found to be potential species. The other gas measured in mass spectrometer could also result due to cracking occurring within the spectrometer, nevertheless the amount of carbon exhaust would still be estimated as the overall amount of pumped out hydrocarbon and oxides of carbon which is about 1 g for OP1.2b.

Table 2. Amounts of carbon detected by DRGA during OP1.2b as hydrocarbons and CO, $CO_2$.

| **Comp -ound** | **Pumped out C from 1 port (g)** | **Fraction (%)** | **Pumped out C from 10 ports (g)** | **Pumped out C during 1256 pulses (g)** |
|---|---|---|---|---|
| CO | $2.32 \times 10^{-5}$ | 27 | $2.32 \times 10^{-4}$ | 0.29 |
| $CO_2$ | $1.56 \times 10^{-5}$ | 18 | $1.56 \times 10^{-4}$ | 0.20 |
| $CH_2$ | $2.20 \times 10^{-5}$ | 25 | $2.20 \times 10^{-4}$ | 0.28 |
| $CH_4$ | $2.58 \times 10^{-5}$ | 30 | $2.58 \times 10^{-4}$ | 0.32 |
| Sum | $8.66 \times 10^{-5}$ | | $8.66 \times 10^{-4}$ | **1.09** |

The amounts of eroded, deposited and pumped out C for OP1.2 are summarized in table 3. It was observed on the TDU marker target measurements that there exists some variation of the erosion pattern along the torus [12] which is due to some misalignment of TDU elements. While these effects are taken into account for the carbon source they could contribute also on the deposition side. However, currently there are not enough data available for any conclusions about the toroidal distribution of deposition. The amounts of carbon exhausted via vacuum pumps during OP1.2a with large C/O impurity concentrations are yet to be estimated.

Table 3. Carbon balance in W7-X.

| Carbon erosion (g) | | Carbon deposition/exhaust (g) | |
|---|---|---|---|
| OP1.2a | 48 ± 14 | Baffle | 23 |
| OP1.2b | 20 ± 6 | Heat shield | 3 |
| Glow discharge | 2.1 | Toroidal closure | 0.2 |
| | | Stainless steel panels | 1.9 |
| | | Plasma vessel wall | 0.3 |
| | | Pumped out | 1.1 |
| Sum | 70.1 ± 20 | Sum | 29.5 |

## 3. Boron balance

### 3.1 Source of boron impurities

For OP1.2b, Boron was injected in W7-X during following two operations:

#### 3.1.1 Boronization

Three boronizations were carried out in W7-X for OP1.2b via glow discharge, using a mixture of He - $B_2H_6$ (diborane) in a ratio of 90%-10%. A total of 147 L mixture was introduced with a cumulative duration of 14 hrs. The spectroscopic observations have shown that these have helped to reduce the C and O impurity concentrations by a factor of 10 and 100 respectively [16, 17], resulting into improved plasma parameters. Considering a density of $B_2H_6$ 1.16 kg/m$^3$, the estimated weight of $B_2H_6$ was 22.85 g (=1.16 kg/m$^3$ * (197 L/10)/1000L/m$^3$ * 1000 g/kg). With a mass fraction of $B/B_2H_6$=0.78, the amount of B introduced was 17.86 g (=0.78*22.85 g). It is assumed that most of the diborane was decomposed in the plasma vessel by the glow discharge. Very small amount of pumped out diborane was decomposed inside a thermal cracking unit. The amount of Boron retained in the thermal cracking unit was not measured.

#### 3.1.2 Boron injection experiments

Another technique to carry out a partial boronization during plasma operation is via boron injector in the midplane manipulator, in which B4C powder is injected during the plasma pulse. This technique was introduced in W7-X for OP1.2b and ca. **2g** $B_4C$ was injected [34]. With a mass fraction of $B/B_4C$=0.78, the amount of B works out to be about 1.6 g (=0.78*2 g).

### 3.2 Deposition of boron

The total amount of B introduced with boronization and boron dropper was 19 g and the corresponding number of B atoms were about 1.1 $x$ 10$^{24}$. Assuming a density of the B/C co-deposit layer 1.4 g/cm$^3$ and the surface area of W7-X PFCs 192 m$^2$ (see table 1), the estimated average thickness of the deposited layer on the PFCs is about 70 nm. Asymmetries will be present.

A couple of first wall tiles removed after OP1.2b were analyzed using ps-LIBS and an average thickness of B rich co-deposition layer of 120 nm was measured [12]. Since 120 nm also include C and O, so that the thickness of B is only about 50-70% of 120 nm. Within the accuracy of these estimates 120 nm and 70 nm are quite comparable. Besides the H/He fuel, the other impurities Fe and Mo originated from the stainless steel areas (see figure 9).

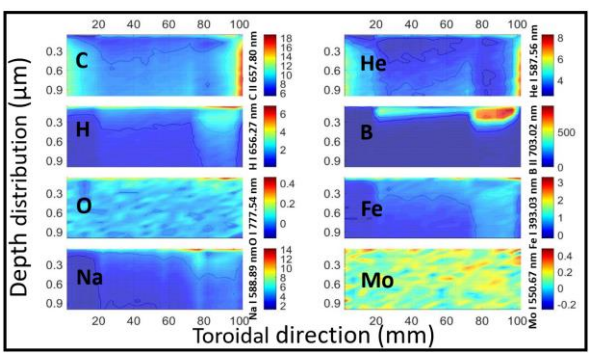


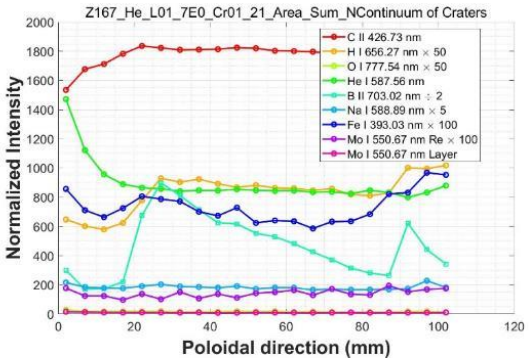

Figure 9. Results of ps-LIBS measurements on a baffle tile (TB-Z167). Figure on the left shows the depth profile of various atoms and on the right, intensities along a poloidal direction are shown.

Considering a homogeneous B deposition layer of 70 nm on all the first wall tiles, the estimated mass of B deposited on various graphite PFC components are (assuming the density of layer, 1.44 g/cm$^3$):

Table 4. Comparison of amounts of boron injected during OP1.2b and deposited on PFCs.

| **Boron injection during OP1.2b (g)** | | **Boron deposition during OP1.2b (g)** | |
|---|---|---|---|
| Glow discharge | 18 | TDU | 2.5 |
| | | Baffle | 3.2 |
| Boron dropper | 1.6 | Heat shield | 4.6 |
| | | Toroidal closure | 0.3 |
| | | stainless steel panels | 0.8 |
| Sum | 19.6 | Sum | 11.4 |

The comparison of B amounts injected during boronization and by using the boron dropper as well as the deposited amount on various first wall components are presented in table 4. The values of introduced and deposited B amounts are comparable.

## 4. Simulations of erosion and impurity migration

### 4.1 Field line tracing modelling of impurity transport

Field line transport code (FLT) is a web-service interface of W7-X, which allows for following field lines, constructing Poincaré maps, estimating heat fluxes to the wall, evaluating magnetic coordinates, etc.. The details of this interface were presented in ref. [35]. FLT was used to estimate the deposition zones of the particles eroded from the TDU strike lines in a single step process ignoring re-erosion and deposition. About 108 000 particles were injected at the strike lines at the horizontal targets of the TDU in half-module 3 lower (HM3*l*) (see figure 10a) in the standard magnetic configuration. It was found that ca. 82% of these particles get deposited on the TDUs, highest of these ca. 31% on the horizontal part of same TDU in HM3*l*. Ca. 14% of the particles were deposited on the baffles of HM2*l* located close to the vertical part of TDU as shown in figure 10b, which provided a possible justification of the thicker deposits with flakes peeling off on the baffle tiles in this location (see figure 10c and 10d). A diffusion coefficient of 1 m$^2$/s was considered for these calculations, a small change ± 0.5 m$^2$/s resulted only in marginal changes of the deposition profile.

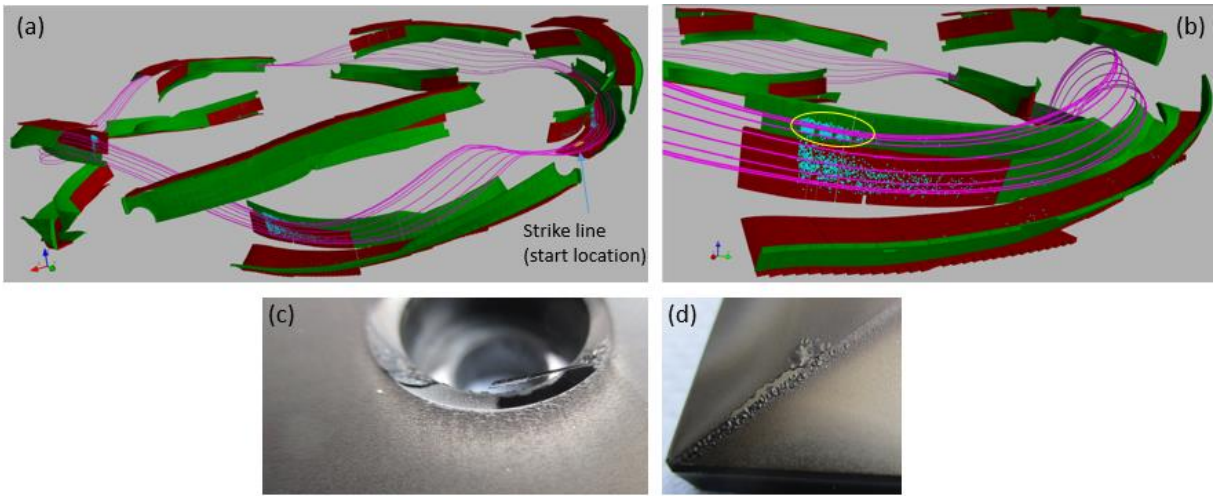

Figure 10. (a) Field line transport estimations by introducing particles on the strike lines in TDU 3l, (b) the deposition on baffles in HM2*l* close to vertical part of TDU, (c and d) high depositions observed on the baffle tiles in the same location. Figure c is at the hole through which the tile is fixed on the support and d is at one of the tile edge.

### 4.2 Erosion/deposition estimations of carbon

In order to analyze the experimentally measured erosion/deposition values for OP1.2b, the estimations of erosion/deposition were carried out using the established relations for the physical and chemical sputtering and redepositions [30, 36]. The net erosion is given by the relation [37]

$$\Gamma_{ero}^{net} = \Gamma_{ero}^{gross} - \Gamma_{redep} = \Gamma_e \frac{(1 - sP_{redep})\Sigma_i Y_i f_i}{1 - P_{redep}(Y_{self} + 1 - s)}$$

Here, $\Gamma_{ero}^{net}, \Gamma_{ero}^{gross}$ : Net, gross erosion. Gross erosion is the overall erosion due to physical and chemical sputtering, net erosion is the remaining erosion after taking the redeposition (by the incident ion flux and prompt redeposition) into account.

$\Gamma_e$ : Electron flux density

$s$: Sticking probability of redeposited impurities

$P_{redep}$: Probability of redeposition

$Y_{self}$ / $Y_i$: Sputtering coefficients due to self/ion sputtering

The incident H and impurity (C, O) ion fluxes (ca. $10^{22}$ ions/m$^2$/s) were estimated from electron density and plasma temperature data measured by the Langmuir probes installed on the nearby targets of TDU 3*l* (lower). The surface temperature of the target was taken from the measured infrared (IR) data. The concentrations of C and O impurities were varied in the range of 4-10% and 0.1-10% respectively. Keeping in mind the surface roughness (see figure 11a), the incident angle was varied from 40°- 60°. The estimated plots of net erosion and deposition along the target for the plasma shot 20180807.014 with incident angles of 40° and 60° are shown in figure 11b. The rate of difference between deposition and erosion at 60° is plotted in figure 11c. The location of highest erosion indicating the location of strike line shows good agreement with the strike line observed with the IR cameras.

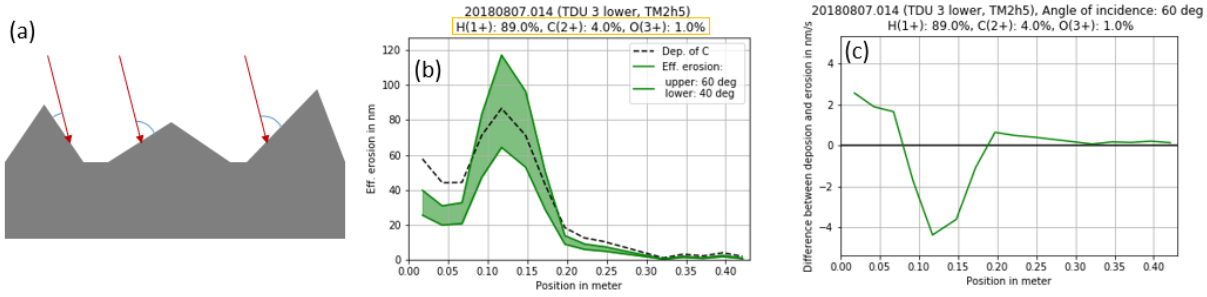


Figure 11. (a) Schematic representation of a rough surface showing the local varying angle of incident ion flux due to the roughness of the target surface, (b) net deposition and erosion for the incident angle of 40° and 60° along a target for the plasma shot 20180807.014, (c) the rate of difference of net deposition with erosion at 60°.

### 4.3 ERO2.0 modelling of carbon erosion and transport

ERO2.0 is a Monte-Carlo code for modelling PWI and 3D plasma edge impurity transport by calculating the test particle trajectories including the full gyro-orbits motions [38]. By parallelizing and including large simulation volumes it is capable of simulating erosion, deposition and material migration for a full 3D fusion device and has been used to simulate PWI in JET [39]. ERO2.0 is being adapted to interpret the erosion/deposition measurements for $^{12}$C in W7-X [17]. The input

plasma parameters such as ion/electron temperatures, ion/heat fluxes were used from EMC3-EIRENE estimations for the standard configuration [40]. The simulation results (see figure 12) show a reasonable match to the measured erosion and deposition pattern on a TDU horizontal targets TM2h6 shown in figure 3. Please note the pumping gap sides are in opposite direction in figures 3 and 12. The plasma strike line at ca. 150 mm from PG and slight deposition at ca. 300 mm appear at similar locations for TM2h6, relatively larger erosion close to PG in ER2.0 deviate from the experimental values due to chemical erosion being over estimated. This is being incorporated in ERO2.0 further. Similar behavior was also observed for TM1h3 and TM3h6 with the marker layer (see figure 12).

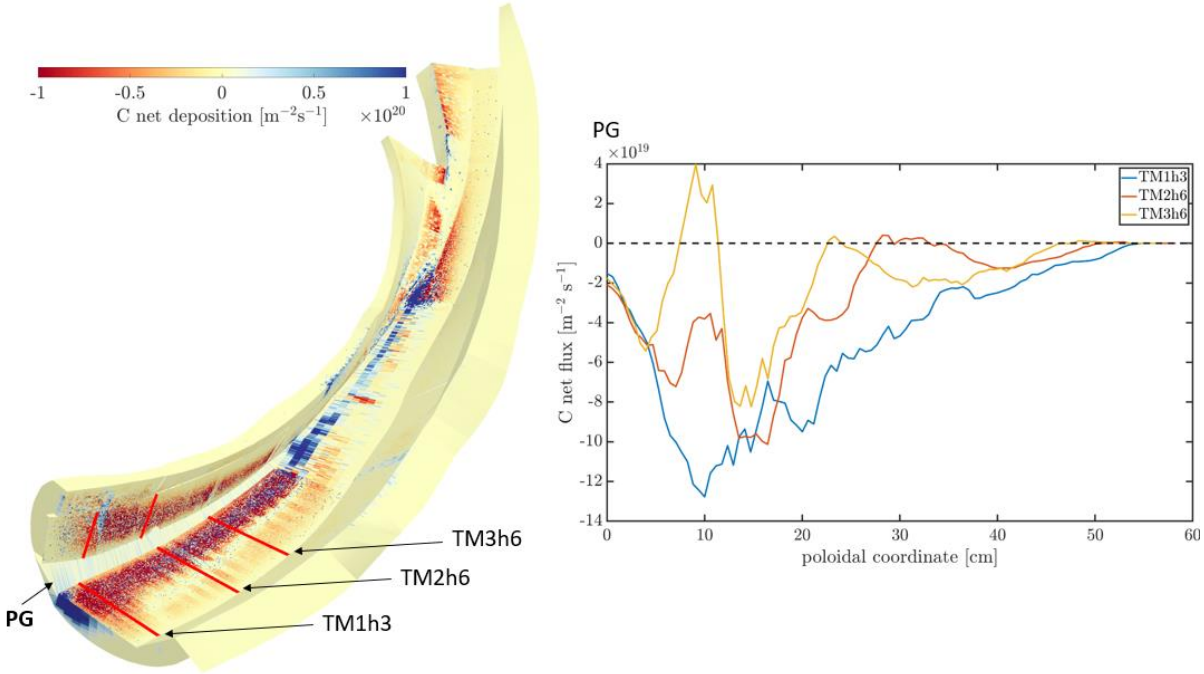


Figure 12. ERO2.0 simulation of erosion and deposition on complete TDU. The erosion and deposition profile along the length of the targets with marker layers TM1h3, TM2h6 and TM3h6 are shown on the right side. The target end at the pumping gap side is marked with PG.

ERO2.0 was used to simulate the depositions observed by EBS measurements on the tile on toroidal closure shown in figures 5c and 5d. The maximum deposition on the closure tile is 6 $x$ $10^{19}$ C-atoms/s/m$^2$ (see figure 13). For the 4809 seconds of operation in standard configuration in OP1.2b [30], the cumulative deposition works out to be 2.9 $x$ $10^{19}$ C/cm$^2$, which is in very good agreement with the black curves for the carbon deposition shown in the figure 5c. However, this estimation is without considering OP1.2a plasma exposure on the modelling side, where standard configuration had 2481 seconds plasma time, probably with higher erosion due to large C and O impurities without boronization. In this case, the modelling might somewhat overestimate the carbon deposition. On the other hand, the above maximum deposition of 6 $x$ $10^{19}$ C-atoms/s/m$^2$ is localized on a small spot on the very edge, on average it's about 3-4 $x$ $10^{19}$ C-atoms/s/m$^2$ at the tile edge, so the agreement appears to be fairly good.

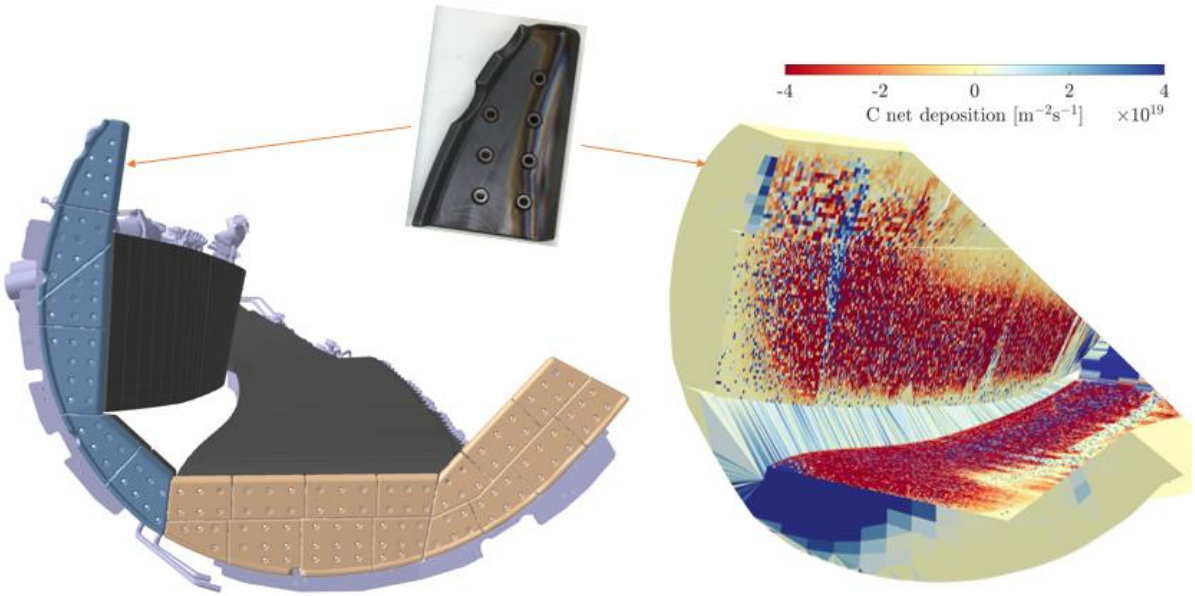


Figure 13. ERO2.0 simulation (figure on the right) of deposition on the toroidal closure tile shown in figure 5d. Figure on the left side shows the location of this tile in the TDU model. The simulation reproduces the deposition pattern measured by EBS (see figure 5c).

## 5. Summary

First efforts were made to understand the carbon balance in W7-X operated with inertially cooled divertor units in OP1.2. At the divertor targets, areas of high net-erosion as well as deposition dominated regions are observed, but net-erosion prevailed considerably. In particular, the strike line regions act as the dominant source of the carbon impurities in the plasma. Rather thick deposited layers with thicknesses >1 µm were observed on some baffle tiles adjacent to the divertor targets. On the heat shield tiles as well as in remote areas, for example on the plasma vessel behind the divertor, only very thin deposits with only few tens of nm thickness were found. This behavior, especially pronounced for OP1.2a, is a profound difference to divertors in tokamaks with carbon plasma-facing components, where the eroded material (from the divertor but also due to erosion at the wall surfaces in the main chamber by charge exchange neutrals) is typically redeposited back onto the divertor targets as well as in remote divertor areas. This may be due to the fact that in W7-X the divertor is not toroidally closed as in tokamaks and higher particle losses can occur during the parallel transport between the different divertor units. This behavior was determined on the basis of limited surface analyses, where different, selected plasma facing components have been taken out after OP1.2b. Moreover, the divertor and the PFCs were not actively cooled and cumulative effects were seen after OP1.2a with high C and O impurity levels and OP1.2b with reduced impurities due to boronizations. Therefore, it would be too early to conclude on a general picture of carbon migration in W7-X. For OP2, a new carbon fiber composite (CFC) divertor is being installed and all the PFCs will be actively cooled, and the input energy to the plasma will stepwise increased to 18 GJ over successive campaigns, the carbon balance will be followed up by in-situ spectroscopic measurements and post-mortem analysis of first wall tiles.

## Acknowledgments

This work has been carried out within the framework of the EUROfusion Consortium and has received funding from the Euratom research and training programme 2014-2018 and 2019-2020 under grant agreement No 633053. The views and opinions expressed herein do not necessarily reflect those of the European Commission. The authors gratefully acknowledge the computing time granted through JARA on the supercomputer JURECA [38] at Forschungszentrum Jülich.

## References

[1] Sunn Pedersen T, Otte M, Lazerson S, Helander P, Bozhenkov S, Biedermann C, Klinger T, Wolf R C, Bosch H -S and the Wendelstein 7-X Team 2016 Confirmation of the Topology of the Wendelstein 7-X Magnetic Field to Better than 1:100,000 *Nature Communications* **7** 13493.
[2] Sunn Pedersen T *et al* 2019 First Results from Divertor Operation in Wendelstein 7-X *Plasma Phys. Controlled Fusion* **61** 014035.
[3] Klinger T *et al* 2019 Overview of first Wendelstein 7-X high performance operation *Nucl. Fusion* **59** 112004.
[4] Dhard C P *et al* 2017 Preparation of erosion and deposition investigations on plasma facing components in Wendelstein 7-X *Phys. Scr.* **T170** 014010.
[5] Dhard C P *et al* 2019 Erosion and deposition investigations on Wendelstein 7-X first wall components for the first phase in divertor configuration *Fusion Eng. Des.* **146** 242.
[6] Brakel R and Sieber T 2021 Private communications.
[7] Alimov V K *et al* 2019 Analysis of mixed-material layers deposited on the toroidal array probes during the FY2012 LHD plasma campaign *Fusion Eng. Des.* **147** 111228.
[8] Oya Y *et al* 2017 Influence of mixed material layer formation on hydrogen isotope and He retention in W exposed to 2014 LHD experiment campaign *Fusion Eng. Des.* **125** 458.
[9] Tokitani M *et al* 2010 Characterization of surface modifications of plasma-facing components in LHD *Fusion Sc. and Tech.* **58** 305.
[10] Motojima G *et al* 2017 Wide-range evaluation of the deposition layer thickness distribution on the first wall by reflection coefficient measurements *Nucl. Mat. Energy* **12** 1219.
[11] Winter J 1996 Wall conditioning in fusion devices and its influence on plasma performance *Plasma Phys. Control Fusion* **38** 1503.
[12] Mayer M *et al* 2020 Material erosion and deposition on the divertor of W7-X, *Phys. Scr.* **T171** 014035.
[13] Zhao D *et al* 2021 Quantification of erosion pattern using picosecond-LIBS on a vertical divertor target element exposed in W7-X *Nucl. Fusion* **61** 016025.
[14] Motojima G *et al* 2020 In-vessel colorimetry of Wendelstein 7-X first wall components: Variation of the layer deposition distribution in OP1.2a and OP1.2b *Phys. Scr.* **T171** 014054.
[15] Mayer M *et al* 2021 Erosion of tungsten marker layers in W7-X *Phys. Scr.* submitted.
[16] Schmid K *et al* 2020 Integrated modelling: Coupling of surface evolution and plasma-impurity transport *Nucl. Mat. Energy* **25** 100821.
[17] Brezinsek S *et al* 2021 Plasma surface interaction in the stellarator W7-X: Conclusions drawn from operation with graphite plasma-facing components *Nucl. Fusion* submitted.
[18] Wang E *et al* 2020 Impurity sources and fluxes in W7-X: from the plasma-facing components to the edge layer *Phys. Scr.* **T171** 014040.
[19] Sereda S *et al* 2020 Impact of boronization on impurity sources and performance in Wendelstein 7-X *Nucl. Fusion* **60** 086007.
[20] Goriaev A *et al* 2020 Wall conditioning at the Wendelstein 7-X stellarator operating with a graphite divertor *Phys. Scr.* **T171** 014063.
[21] Eckstein W, Garcia-rosales C, Roth J and Ottenberger W, 1993 Sputtering data, IPP Report 9/82.
[22] Dhard C P *et al* 2020 Inspection of W7-X plasma-facing components after the operation phase OP1.2b: observations and first assessments *Phys. Scr.* **T171** 014033.
[23] Pardanaud C, Martin C and Roubin P 2017 Raman Spectroscopy and Applications (Intertech open science | open minds) Chapter 1 http://dx.doi.org/10.5772/65649 .
[24] Pardanaud C *et al* 2011 Raman study of CFC tiles extracted from the toroidal pump limiter of Tore Supra *J. Nucl. Mater.* **415** S254.
[25] Tsitrone E *et al* 2009 Deuterium inventory in Tore Supra: reconciling particle balance and post-mortem analysis *Nucl. Fusion* **49** 075011.
[26] Richou M *et al* 2007 Physio-chemical characteristics of carbon deposits collected in TEXTOR and Tore Supra tokamaks *Carbon* **45** 2723.
[27] Balden M *et al* 2014 Collection strategy, inner morphology, and size distribution of dust particles in ASDEX Upgrade *Nucl. Fusion* **54** 073010.
[28] Hwangbo D *et al* 2020 Inspection of Arc Trails formed in stellarator/heliotron devices W7-X and LHD *Plasma and Fusion Research* **15** 2402012.
[29] Schlisio G *et al* 2019 First results from the implementation of the ITER diagnostic residual gas analyzer prototype at Wendelstein 7-X *Rev. Sci. Instrum.* **90** 093501.
[30] Roth J and Garcia-Rosales D 1997 Analytical description of the chemical erosion of graphite by hydrogen ions, Corrigendum *Nucl. Fusion* **37** 897.

[31] Küppers J 1995 The hydrogen surface chemistry of carbon as a plasma facing material *Surf. Sci. Rep.* **22** 249.
[32] Horn C *et al* 1994 H atom impact induced chemical erosion reaction at C:H film surfaces *Chem. Phys. Lett.* **231** 193.
[33] Rai A *et al* 2010 Modeling of chemical erosion of graphite due to hydrogen by inclusion of chemical reactions in SDTrimSP *Nuclear Instruments and Methods in Physics Research B* **268** 2639 and the references therein. http://dx.doi.org/10.1016/j.nimb.2010.06.040
[34] Lunsford R *et al* 2021 *Phys. Plasmas* submitted.
[35] Bozhenkov S A *et al* 2013 Service oriented architecture for scientific analysis at W7-X. An example of a field line tracer *Fusion Eng. Des.* 88 2997.
[36] Chodura R 1982 Numerical analysis of plasma-wall interaction for an oblique magnetic field *J. Nucl. Mat.* **111-112** 420.
[37] Naujoks D 2006 Plasma-Material Interaction in controlled Fusion (Springer Series on Atomic, Optical and Plasma Physics Vol 39 Chapter 12 Springer Verlag, Berlin, Heidelberg, New York.
[38] Jülich Supercomputing Centre 2018 JURECA: Modular supercomputer at Jülich Supercomputing Centre *Journal of large-scale research facilities* **4** A132. http://dx.doi.org/10.17815/jlsrf-4-121-1
[39] Romazanov J *et al* 2019 Beryllium global erosion and deposition at JET-ILW simulated with ERO2.0 *Nucl. Mater. Energy* **18** 331.
[40] Effenberg F *et al* 2019 First demonstration of radiative power exhaust with impurity seeding in the island divertor at Wendelstein 7-X *Nucl. Fusion* **59** 106020.